Assessment of Radioactive Cesium Contamination in Concrete Structures near Fukushima Daiichi Nuclear Power Plant

Kazuo Yamada[1], Hiroyuki Arai[1], Ippei Maruyama[2], Kazutoshi Shibuya[3], Kazuto Endo[1]

*1 Fukushima Regional Corporative Research Center, National Institute for Environmental Studies

*2 Department of Engineering, The University of Tokyo

*3 Taiheiyo Consultant Co. Ltd.

Abstract

This study investigates the contamination of concrete by radioactive cesium released by the Tokyo Electric Power Company Fukushima Daiichi Nuclear Power Plant accident using samples from various sites in the town of Okuma, Japan. Concrete contamination was effectively evaluated through surface dose rate measurements using Geiger-Müller tubes with shielding. Corresponding radioactivity concentrations were evaluated using an NaI scintillator in a low background environment. The contamination levels were considerably lower in areas shielded from rain compared with outdoor areas exposed to rain. Contamination within concrete can be primarily attributed to radioactive Cs enrichment in specific concrete aggregates and further influenced by carbonation of the cement paste. In non-carbonated sections, radioactive Cs was concentrated in aggregates near the surface, hindering the penetration of detection into the cement paste. Concrete samples subjected to rain exhibited reduced contamination over time. Thus, rain exposure, aggregate properties, and the degree of carbonation emerged as pivotal in predicting concrete contamination. Therefore, this study yields insights into on-site measurement methods, temporal contamination trends in the environment, and the distribution of contamination within concrete structures.

Keywords： cesium contamination, concrete carbonation, aggregate

1. Introduction

The Fukushima Daiichi Nuclear Power Plant (1F) operated by Tokyo Electric Power Company (TEPCO) experienced a catastrophic accident during the Great East Japan Earthquake on March 11, 2011, leading to widespread contamination of eastern Japan, primarily by radioactive cesium (Fig. 1; [1]). The contamination of various types of concrete from off-site localities close to 1F was investigated in our previous study [2]. Further evaluation of contamination levels within concrete structures is crucial for discerning the migration of radioactive Cs within concrete pits utilized for the disposal of radioactively contaminated waste and further aiding the demolition of the 1F buildings.

Previous studies have reported on post-accident concrete contamination at nuclear facilities such as the Chernobyl nuclear power plant (ChPP) [3], the Three Mile Island nuclear power plant (TMI) [4], and 1F [5]. Analysis of concrete with epoxy coatings at building 1F has revealed that contamination is confined solely to the epoxy surface layer but does not permeate deeper within the concrete structure [5], consistent with results for TMI. In the ChPP case study, core samples were collected from the exterior wall section of a 6-story reinforced concrete building and analyzed to a depth of 5 mm [3]. The contamination level decreased by 90% within 5 mm of the surface. Similarly, high contamination levels were confined to depths of a few centimeters in paint cracks at TMI [4].

In a previous study [2], we demonstrated that contamination can penetrate concrete up to 10 cm along existing cracks, a phenomenon hitherto unreported. The penetration of radionuclides into concrete under saturated conditions, such as those encountered in turbine pit basements, have been actively investigated through experiments under the Japanese Ministry of Education, Culture, Sports, Science, and Technology (MEXT) “Wisdom Project” [6,7,8,9].

Experimental studies have revealed that Cs penetration into concrete is notably influenced by the constituents of the concrete (particularly concrete aggregates with Cs adsorption properties) as well as the state of deterioration (notably neutralization and Ca dissolution) and the contamination environment (in which potassium may competitively adsorb against Cs) [9].

The ChPP incident involved a reactor core explosion, dispersing various fission products (FPs), while at the TMI, contamination resulted from core cooling water containing boric acid from the pressurized water reactor seeping into the concrete. By contrast, at 1F, the turbine building basement was initially flooded by the tsunami and subsequently exposed to a mixture of core water and seawater injected for core cooling, leading to contamination by water-soluble FPs. The effects of boric acid were limited because of the core water composition of the boiling water reactor and its mixing with seawater. Within the upper structures of the F1 building, leaks from the core periphery released the primary volatile elements as aerosols,

https://doi.org/10.26434/chemrxiv-2024-bqr88 ORCID: https://orcid.org/0000-0001-5835-8636 Content not peer-reviewed by ChemRxiv. License: CC BY-NC-ND 4.0

depositing them within the building through piping ducts, and outdoors were contaminated with rain fall. Given this contamination process, radioactive Cs emerges as the primary radionuclide contributing to the ongoing contamination [10] in upper structure components. Therefore, each concrete contamination scenario is unique and depends on the accident circumstances, concrete condition, and contamination history.

The large volume of concrete at 1F (estimated at approximately 800,000 m^3 [6]) necessitates the evaluation of contamination status and effective management, decontamination, storage, and disposal based on precise assessments of radioactivity concentration [11]. Contamination, often penetrating deeply along cracks (up to 10 cm depending on crack density [9]), poses formidable challenges to decontamination and potential reuse. Consequently, demolition emerges as the final stage of decommissioning, and sufficient time must be allowed for its execution. However, certain superstructure components of 1F are planned to be demolished earlier to facilitate the removal of molten fuel debris. The air dose rate at 1F, notably lower in the superstructures compared with the significantly contaminated underground structure [12], demands earlier contamination estimation for the less contaminated superstructures. Despite over 100 measurements [13], the contamination status of 1F concrete has yet to be comprehensively evaluated.

For the above reasons, this study performed a comparative analysis of the contamination results of concrete surveyed at various locations across Okuma town and buildings adjacent to 1F. The surveyed concrete, predominantly exposed to outdoor environments, exhibited considerable variation in contamination levels. For example, concrete affected by the tsunami included collapsed columns, upright columns, and rubble, which may or may not have been stripped of surface concrete, may or may not contain cracks, and may have been altered by rain differently. Furthermore, temporal variations in contamination were observed at the same sites. Structural concrete examination revealed the emergence of various phenomena that cannot be predicted solely through laboratory experiments. This paper discusses the crucial factors for predicting contamination levels realistically.

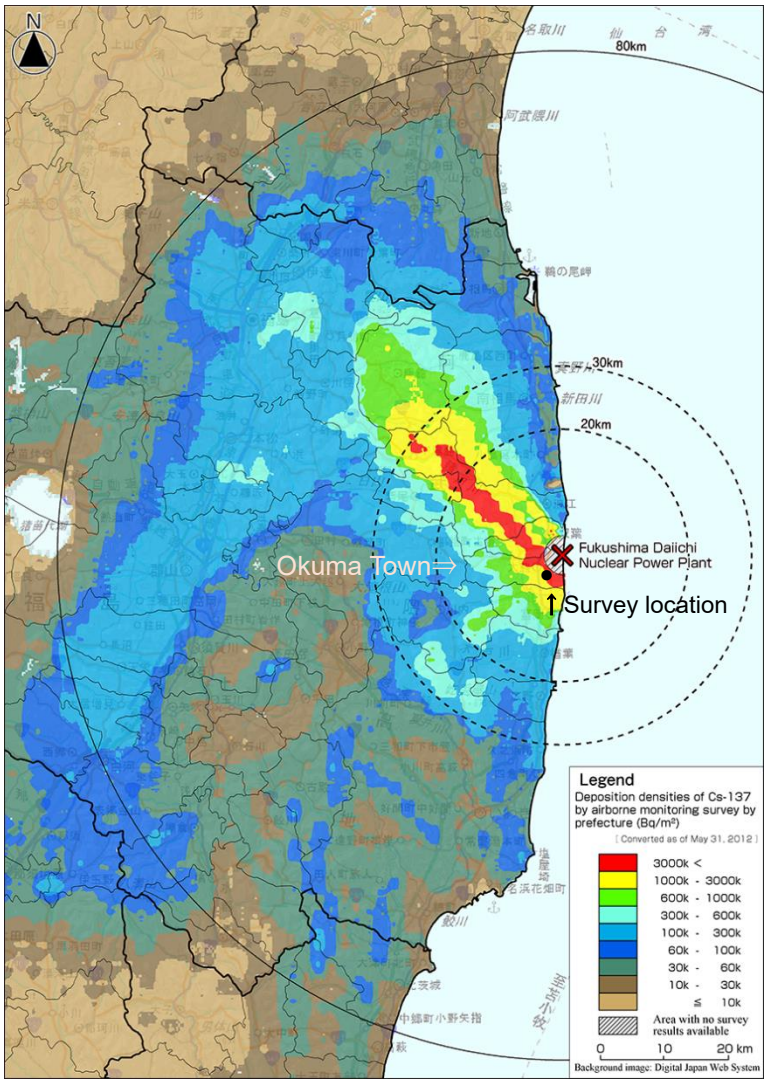

Fig. 1 Air dose rate map around building 1F [1] and the survey area, with sampling locations.

https://doi.org/10.26434/chemrxiv-2024-bqr88 **ORCID:** https://orcid.org/0000-0001-5835-8636 Content not peer-reviewed by ChemRxiv. **License:** CC BY-NC-ND 4.0

2. Field survey and analysis

(1) Survey periods

This paper summarizes the results of four distinct surveys. The first survey was conducted on December 2, 2014, at several locations in Okuma town. The primary objective was to conduct a general survey of contamination levels at each location.

The second survey was conducted on December 2-3, 2015, focusing on the structure of the former Fukushima Prefecture Fish Farming Experimental Station, which was located approximately 500 m south of the southern boundary of the 1F site. The station was situated a few meters above sea level, overlooking the Pacific Ocean. The measurements focused on the contamination of rubble and the effects of cracks.

The third survey was conducted on October 27, 2017 at the same location as the 2015 survey. Core samples were extracted from different sections of the building for analysis.

Finally, the fourth survey was conducted on January 17, 2024, at the same location as the 2015 and 2017 surveys. The aim was to assess temporal changes in surface dose rates and contamination depths.

(2) Location of the surveys

The first survey was conducted at several sites across Okuma Town with varying air dose rates (Fig. 1). These sites included concrete lids of road gutters, pavement concrete around buildings, building columns (described in the next section), and concrete construction blocks. Surface dose rates were measured in the field using Geiger-Müller (GM) tubes, while radioactivity concentrations were determined on crushed core samples at the National Institute of Environmental Studies laboratory in Tsukuba City, which is a low radiation background laboratory.

The facility surveyed in the second through fourth stages is described in more detail here, and the sampling locations are indicated in the next section. The facility is a dome-shaped building, which featured a circular pool for flatfish farming. The building endured severe damage during the March 11, 2011 tsunami, half of the building on the seaward side having collapsed (Fig. 2). Additionally, a neighboring one-story reinforced concrete building suffered partial destruction, including the collapse of a wall (Fig. 3).

Fig. 2 Collapse of the dome-shaped building during the tsunami.

https://doi.org/10.26434/chemrxiv-2024-bqr88 **ORCID:** https://orcid.org/0000-0001-5835-8636 Content not peer-reviewed by ChemRxiv. **License:** CC BY-NC-ND 4.0

Fig. 3 One-story building with collapsed walls and rubble.

(3) Sample collection sites in the 3rd and 4th surveys

Samples were collected from rubble and debris of collapsed concrete buildings (Fig. 4) and from intact concrete structures. The intact structures included a column that was cracked by the tsunami but was standing upright (Fig. 5a), a collapsed column (Fig. 5b), a collapsed column with a spalled concrete cover (Fig. 5c), the floor of the facility (Fig. 5d), and the bottom of the aqua-farming pond (Fig. 5e).

Fig. 4 Example of rubble.

https://doi.org/10.26434/chemrxiv-2024-bqr88 **ORCID:** https://orcid.org/0000-0001-5835-8636 Content not peer-reviewed by ChemRxiv. **License:** CC BY-NC-ND 4.0

(a) Upright columns that survived the collapse of the building

(b) Building columns that collapsed during the tsunami

(c) Columns that had collapsed and whose cover concrete was spalled

https://doi.org/10.26434/chemrxiv-2024-bqr88 **ORCID:** https://orcid.org/0000-0001-5835-8636 Content not peer-reviewed by ChemRxiv. **License:** CC BY-NC-ND 4.0

(d) Floor of the building containing the flatfish farming pond

(e) Bottom of aqua-farming pond

Fig. 5 Core sampling locations.

(4) Surface dose rate measurement

Surface dose rates for radioactive Cs were measured using two types of survey meter: an NaI scintillator type meter (NaI, TCS-172B, ALOKA) and GM tube type meter (TGS-146B, ALOKA). A 8.4-kg lead cylindrical shield was employed to minimize environmental radiation effects. Measurements were conducted with the surface of the detector protected by a plastic film and meters were in direct contact with the sample under examination. NaI meters predominantly detect gamma-rays, which have a greater penetration depth so that signals are assessed not only from the surface layer of the sample but also from deeper parts (up to roughly 10 cm). GM tubes primarily detect beta-ray radiations which has a shorter depth penetration range, providing radiation readings at the sample surface. The effectiveness of the shielding is expected to be relatively high.

(5) Core sampling

The depth of radioactive Cs penetration can be estimated to some degree from the relationship between on-site GM tube and NaI measurements [2]. However, estimation through this method is challenging when the dose rate in the surface layer is

https://doi.org/10.26434/chemrxiv-2024-bqr88 **ORCID:** https://orcid.org/0000-0001-5835-8636 Content not peer-reviewed by ChemRxiv. **License:** CC BY-NC-ND 4.0

considerably higher than that of deeper layers or when Cs penetration is inhomogeneous. Therefore, cores with diameters of 47 mm and 50 mm were collected in the second and third surveys and the fourth survey, respectively, through core drilling using water-lubricated core bits. Given the outdoor exposure of the samples to rainfall over several years, the impact of water usage during drilling was considered negligible. The sampling process is shown in Figs. 5a-c.

Radioactive Cs penetration into the collected cores was assessed by cutting the cores along their length (*i.e.*, depth). Cores obtained during the second survey were cut using a dry wire saw [2], but subsequent surveys employed a water-cooled diamond wheel saw for in-field cutting because of operational inefficiency and substantial dust generation by the dry-wire saw.

(6) Radioactivity concentration measurement

Radioactivity concentration of radioactive Cs was measured using a Ge-type detector (ORTEC GMX-15190) for Cs-137 and Cs-134. The total concentration was measured without decay calibration. The concrete samples were crushed to particles of sizes less than 1.25 mm under homogeneous conditions and several 10s grams of samples were placed in 100 cm^3 plastic vessels (U-8 vessels).

In cases where contamination was predicted only for the aggregate portion, a small sample was ground from the aggregate using a milling machine equipped with a 10-mm diameter drill bit. Considering that the precision of the quantification is uncertain because of the small sample quantity, a simple quantification was performed based on the peak intensity of each radionuclide.

(7) Radioactive contamination depth measurement

The cut surfaces of the core, from which the Cs-137 depth profile was obtained, were evaluated through autoradiography with imaging plates (IPs). Measurements were conducted on the surface of the original structure and on two or three depth-segmented surfaces of the core.

The radioactivity distribution was evaluated by simultaneously exposing a cement paste (cylindrical shape with a diameter of 20 mm and a height of 10 mm) containing 1 MBq/kg of Cs-137. All samples were placed on an IP (GE Healthcare MS2025) for measurements over different time durations, with the sample surfaces protected by thin plastic film. After exposure, the IP was loaded into a signal reading holder in a dark room. A GE Healthcare Typhoon FLA7700 was used for signal reading. The collected data were converted into a two-dimensional quantitative map using Image Quant V.8.2 (GE Healthcare).

3. Results

(1) Surface dose rate

The surface dose rate measurements of structural concrete and rubble obtained during the first survey are depicted in Figs. 6 and 7, respectively. Ideally, a 1:1 linear relationship is expected for each measurement method, irrespective of shielding presence, in the absence of external environmental influences. However, as shown in Fig. 6, a comparison of the two methods, particularly with NaI, revealed poor correlation because of significant variation, with unshielded measurements yielding higher values in some cases. In addition, the effectiveness of shielding exhibited substantial variability across measurement locations because of difference air dose rates. As shown in Fig. 7, the measurements using the unshielded GM tube yielded larger values but with relatively good linearity for shielded measurements.

Fig. 6 illustrates an overall linear relationship between respective dose rates when data are grouped based on shielding presence, although γ-rays cannot be entirely shielded, leading to variation. However, certain measurement locations, delineated by red circles, indicated considerably elevated values in the absence of shielding, attributable to increased air dose rates. One contributing factor could be the presence of soil. As experienced in decontamination works in off-site, at the place where rainwater directly drained from gutters to the ground exhibited locally quite higher dose rates even during off-site decontamination efforts [13]. This phenomenon arises from the adsorption of radioactive Cs by soil, with rainwater containing radioactive Cs increasing its concentration upon continuous supply. Although the surveyed facility predominantly comprises concrete-covered areas, grass growth from the soil was observed in some regions; the points encircled in red indicate areas influenced by soil radiation. Excluding these data points, the correlation coefficient R^2 between values with and without shielding increased from 0.42 to 0.75. Additionally, shielding resulted in a reduction of counts by 5 μSv/h (y-intercept of the regression line), equivalent to 36% of the maximum value of 18 μSv/h.

Fig. 7 shows the relationship between GM tube readings with and without shielding. The correlation coefficient R^2 of 0.97 indicates strong linearity, with shielding reducing readings by an average of 2 kcpm. This reduction, accounting for 10% of the maximum value of 23 kcpm, represents a fraction of the effect observed with NaI. Essentially, β-ray measurements exhibit relatively low sensitivity to variations in air dose rates at measurement sites. Among fission products, Cs-134 and Cs-137

https://doi.org/10.26434/chemrxiv-2024-bqr88 **ORCID:** https://orcid.org/0000-0001-5835-8636 Content not peer-reviewed by ChemRxiv. **License:** CC BY-NC-ND 4.0

emitting β and γ rays and Sr-90 emitting β rays, primarily influence dose rates. Typically, GM tubes detect β-rays from these nuclides. However, in scenarios where contamination is primarily attributed to radioactive Cs, as observed at the 1F off-site locality [10], GM tube assessments offer a more appropriate gauge of contamination levels due to their lower sensitivity to air dose rate when shielding is applied.

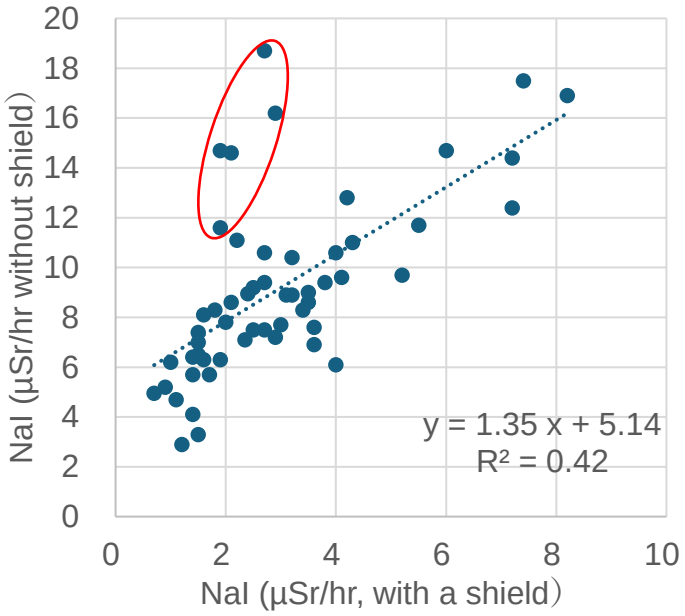

Fig. 6 γ-ray dose rate measurement by NaI scintillator in the filed.

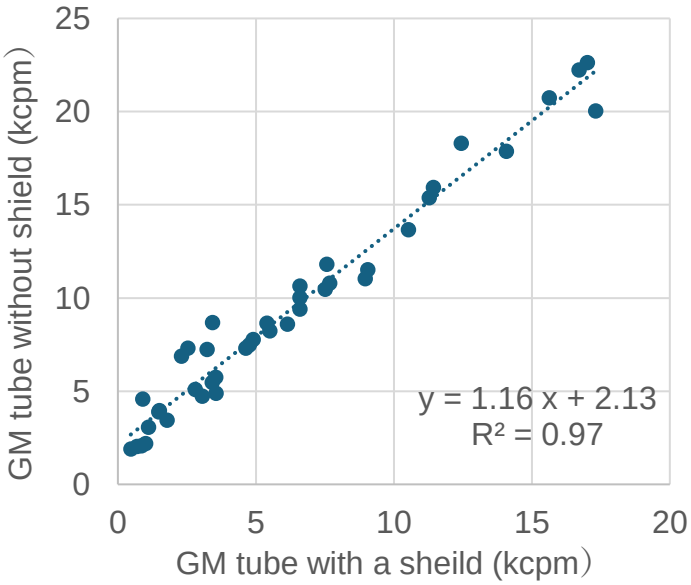

Fig. 7 β-ray dose rate measurement by GM tube in the field.

The rubble samples (from the aqua-farming facility) obtained during the third survey were transported to the laboratory at the National Institute for Environmental Studies in Tsukuba City for surface dose rate measurements. In the sample storage room, the air dose rate was 0.07 μSv/h for NaI and 72 cpm for GM tube. The correlation between NaI and GM tube measurements was plotted for field conditions (with shielding) and laboratory conditions (without shielding), respectively. The correlation coefficient R^2 was 0.60 for the field measurements and 0.89 for the laboratory measurements. The better correlation observed for the laboratory data suggests that field measurements were influenced by radiation from the surrounding area. The linearity between the NaI and GM tube readings indicated that, for the evaluated samples, most radioactive Cs was concentrated near the sample surface, where β-rays remain unattenuated and penetration into the interior of the sample is limited.

https://doi.org/10.26434/chemrxiv-2024-bqr88 **ORCID:** https://orcid.org/0000-0001-5835-8636 Content not peer-reviewed by ChemRxiv. **License:** CC BY-NC-ND 4.0

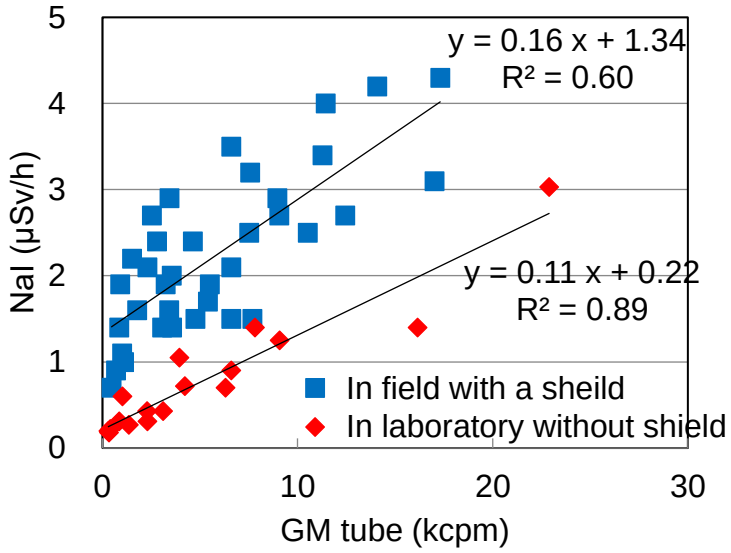

Fig. 8 Correlation of GM tube and NaI measurements in field with a shield and in laboratory environments without shield

Because of the polyhedral structure of the rubble, rainfall-induced contamination may vary across the top, side, and back surfaces. Therefore, several blocks of rubble (10 cm to 30 cm in length) were tested at each side while employing on-site shielding. The results are summarized as a histogram in Fig. 9. The mode and maximum values were 9 kcpm and 24 kcpm for the top surface, 3 kcpm and 9 kcpm for the sides, and 3 kcpm and 6 kcpm for the back surface, respectively. Contamination levels were notably higher on the top surface compared with the sides, with the back surface exhibiting even lower contamination levels. However, the determination of differences in contamination between the sides and the back is challenging because of the limited number of measurements on the back side.

Only one measurement of the contamination level inside the half-collapsed building was made because of the risk of collapse of components within the structure. The readings were 0.7 μSv/h for NaI and 0.5 kcpm for GM tube, the lowest among all measurement points.

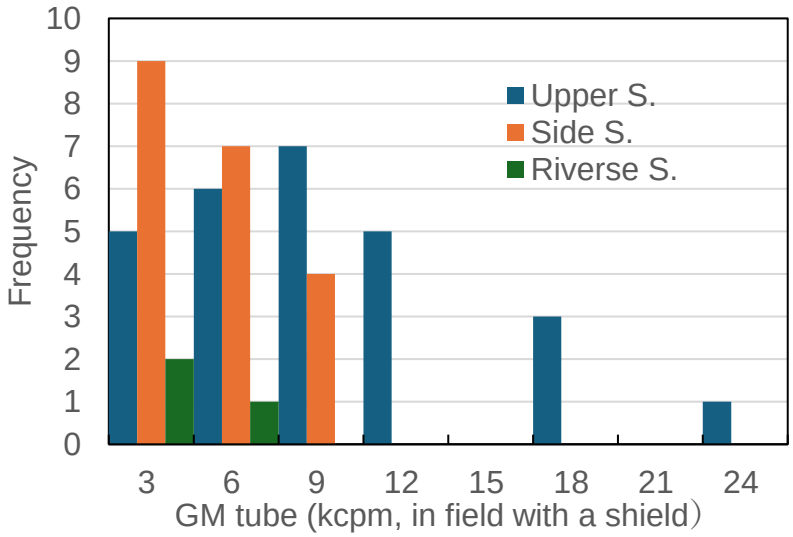

Fig. 9 Difference of dose rate frequency depending on the direction of concrete rubble.

https://doi.org/10.26434/chemrxiv-2024-bqr88 **ORCID:** https://orcid.org/0000-0001-5835-8636 Content not peer-reviewed by ChemRxiv. **License:** CC BY-NC-ND 4.0

(2) Radiation concentration

Although the radiation dose rate is crucial for managing on-site exposure, radioactivity concentration is more important when considering disposal. Therefore, the cores collected in the initial survey were crushed and evaluated for Cs-134 and Cs-137 using a Ge detector. The values apply to June 3, 2015. Given that the majority of radioactive Cs is expected to be located in the surface layer, the radioactivity was divided by the area of the core with a diameter of 47 mm to give surface radioactivity concentration. The ratio of Cs-134 to Cs-137 was established at 0.274, with a stable variation of 3%, indicating satisfactory measurement accuracy.

Fig. 10 shows the relationship between surface radioactivity concentration and measured values using GM tube with a shield in the field or NaI, which were deemed suitable for measuring total γ-ray radioactivity in a low background environment. A robust linear relationship between surface radioactivity concentration and laboratory NaI counts was observed, with a correlation coefficient R^2 of 0.97. While a positive correlation was observed between measured values and radioactivity level with GM tubes, the variation was substantial, as indicated by a y-intercept of 6 kcpm and R^2 of 0.77. Fig. 8 shows a high correlation between NaI and GM tube measurements in a low background environment, indicating that GM tube measurements in the field may be moderately influenced by the air dose rate at the measurement site.

Using the regression equation, GM tube counts were converted into estimates of surface radioactivity concentration (Fig. 10), revealing an average difference of 76 Bq/cm^2 from the measured values. This value is considered as an estimation error in this study. The error in determining radioactivity density from NaI in the laboratory was 24 Bq/cm^2. The dotted line in Fig. 10 represents twice the error, indicating the range of estimation from survey meter readings. Because of the relatively large error associated with estimating radioactivity density from field measurements using GM tubes, for more accurate estimation, the radioactivity concentration of core samples is recommended to be assessed in the laboratory using NaI. Note that radioactive Sr was not evaluated in this analysis.

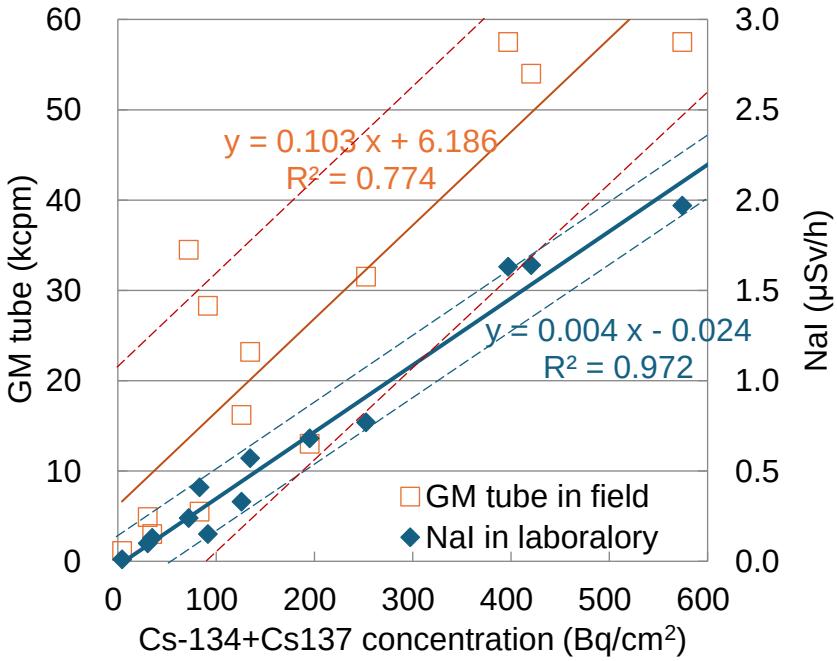

Fig. 10 Correlations between GM tube measurements in the field with a shield or NaI measurements in the laboratory versus radioactive Cs surface concentration.

(3) Changes in surface dose rate over time in the field

Field measurements of aqua-farming facility columns were conducted twice, once in the second and again in the fourth surveys. Fig. 11 shows two examples of columns measured at the same location. The values were adjusted to reflect the conditions on March 11, 2011, accounting for attenuation effects. In Fig. 6, only a low correlation between NaI and GM tube data was observed. However, in Fig. 11, a high correlation between NaI and GM tube data was observed for both collapsed and upright columns, indicating consistent air dose rates at the same location.

Examining results for the collapsed column in Fig. 11a, both GM tube and NaI readings were reduced by half in January 2024, approximately 8 years later, compared with measurements conducted in December 2015. This reduction could signify the leaching of radioactive Cs into the environment due to rain. Measurements above cracked surfaces were greater than those

https://doi.org/10.26434/chemrxiv-2024-bqr88 **ORCID:** https://orcid.org/0000-0001-5835-8636 Content not peer-reviewed by ChemRxiv. **License:** CC BY-NC-ND 4.0

in the crack-free areas in December 2015, but no clear difference was observed in the January 2024 measurements. The reason for this is not well understood.

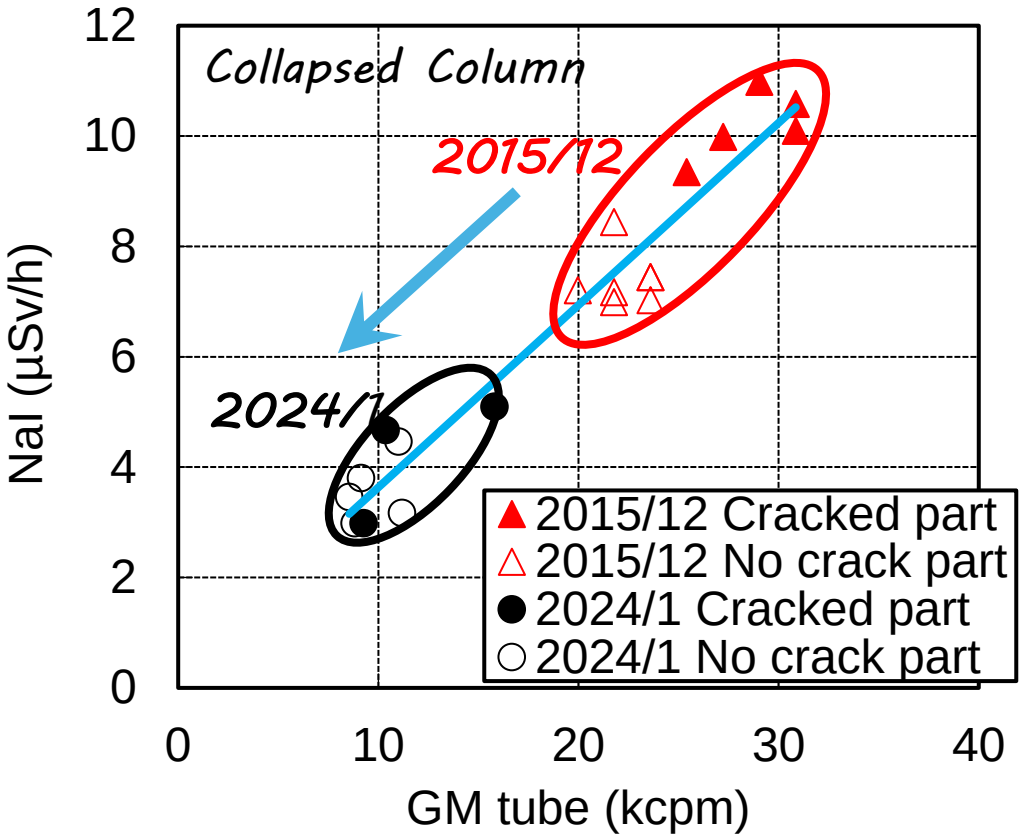

(a) Collapsed column with cracks.

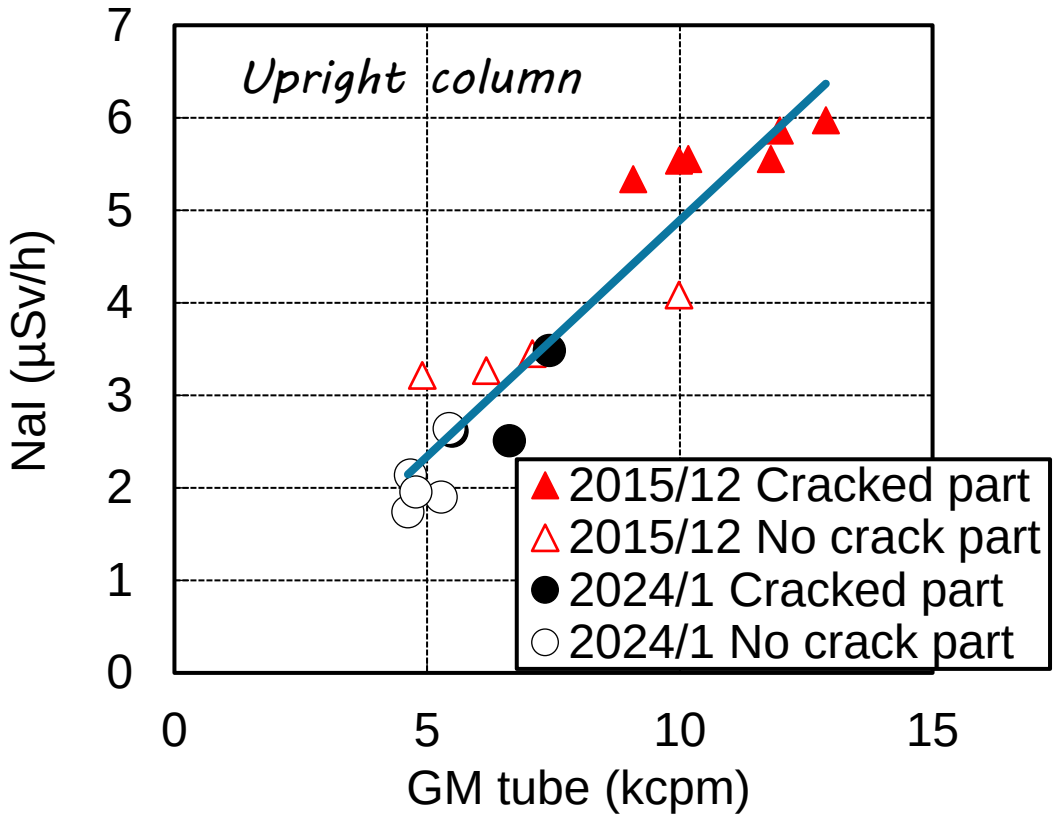

(b) Upright column with cracks caused by the tsunami.

Fig. 11 Changes in radiation dose rate of columns from December 2015 to January 2024. Dose rates were calibrated for the values on March 11, 2011.

https://doi.org/10.26434/chemrxiv-2024-bqr88 **ORCID:** https://orcid.org/0000-0001-5835-8636 Content not peer-reviewed by ChemRxiv. **License:** CC BY-NC-ND 4.0

Fig. 11b depicts results for an upright column on the north face, facing to the 1F site. Compared with the collapsed column, the measured values were approximately half. This aligns with the trend observed for rubble in Fig. 9, where the top surface exposed to rainwater remained highly contaminated. Over time, the contamination levels decreased substantially, which is particularly evident in cracked parts where the dose rate was halved. On the other hand, while the dose rate decreased in areas without cracks, the reduction was not as substantial as in the cracked parts. The surface dose rate also decreased with age in both collapsed and upright columns.

(4) Changes in radioactive Cs distribution over time during storage

Samples collected in December 2015 during the second survey were stored in plastic bags until November 2016, when the cores were dry cut, and IP measurements of the cross sections were conducted [2]. Subsequently, the samples were placed in plastic bags again and stored in SUS containers of 20 L volume with other concrete samples in a storage facility. The temperature and humidity of the storage facility was not controlled. The humidity in the container was 50 %RH in May 2024. In February 2024, the samples were removed and re-measured.

Fig. 12 shows cross-sectional autoradiographs of cores from a collapsed column with a crack (left) and an upright column with a crack (right). The top images were captured in November 2016 [2], while the bottom images were captured in February 2024. While the intensity decreased because of radioactive decay of Cs-134 and Cs-137, their distribution remained consistent, with no discernible traces of migration.

Under dry conditions, radioactive Cs exhibited minimal migration detectable by IP-based evaluation. Although previous measurements have revealed Cs reduction from the surface upon exposure to outdoor rainwater, Cs concentration was constant in dry environments.

In a simple cement paste specimen, we reported that Cs-137 moved during drying [15]. Cs-137 was concentrated around the disks over time, when 1 MBq/kg of Cs-137 was added to ordinary Portland cement paste having 0.50 of water-to-cement ratio, using a solution with a radioactivity concentration of 200 kBq/mL and a CsCl concentration of 0.05 mass%, and processed into disks with a diameter of 2 cm and a thickness of 1.6 mm, covered on both sides with Mylar membrane and Al tape [15]. This concentration phenomenon might be attributed to slight water migration during the weeks to months after molding. Cement paste typically consists of calcium silicate hydrate with a high Ca/Si ratio and contains large amounts of Na and K, which interact minimally with Cs. Therefore, Cs, being an alkali metal, is assumed to migrate along with the water. As water migration decreases over longer time scales, the migration of Cs may also cease.

Radioactive Cs did not exhibit mobility within concrete as shown in Fig. 12 because, besides the above reason, Cs is absorbed and immobilized in certain types of aggregates within the concrete [16], preventing migration under sealed indoor conditions. When Sr-90 was introduced into cement paste, the concentration distribution of Sr-90 remained uniform over time, with no observable concentration gradients [15]. Similarly, no migration concentrations were observed over time when Cs-137 was sprayed on river gravel crushed material and molded with epoxy resin. Cs-137 migrated only within the neat Portland cement paste.

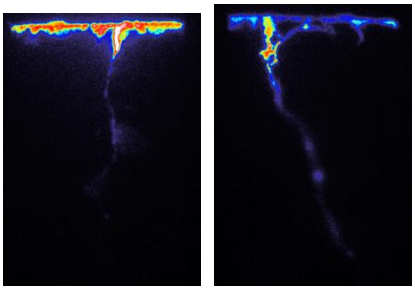
November 2016

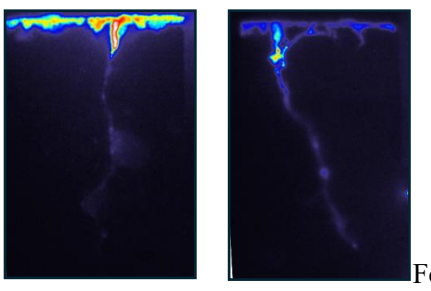
Feburary 2024

https://doi.org/10.26434/chemrxiv-2024-bqr88 **ORCID:** https://orcid.org/0000-0001-5835-8636 Content not peer-reviewed by ChemRxiv. **License:** CC BY-NC-ND 4.0

Collapsed column　Upright column

Fig. 12 Autoradiographs of the cross-section of sampled cores containing cracks from concrete columns. The left side shows a collapsed column, and the right side shows a upright column. The upper images were captured in November 2016 with an exposure time of 48 h, and the lower images were captured in February 2024 with an exposure time of 23 h. The core diameter is 47 mm.

(5)　Contamination of cores from different positions

Images of the exterior of six concrete cores collected from different building locations during the third survey are shown in Fig. 13. These sites include an upright column, a collapsed column which had lost concrete cover, a cracked floor surface coated with anti-slip sand-containing resin within the facility, and the cracked bottom surface of the aqua-farming pond with some coating. The width of the sample from floor was 1 mm and that of the sample from pond bottom was 0.2 mm.

Fig. 14 shows the IP images of the core surfaces, representing the concrete surfaces within the structure. The collapsed columns whose concrete cover had been lost were excluded from measurement due to surface irregularities. Within the surface layer of the upright columns, scattered areas exhibit spotty high radiation dose rates. Although correlating these areas with the optical image of the surface in Fig. 13 is challenging, it is hypothesized that the concentration in the aggregate areas is high, with some degree of adsorption in other cement paste areas [9].

On the other hand, contamination levels were low for the facility floor and remained at background levels even when the contrast was increased by a factor of 5. Similarly, the bottom of the aqua-farming pond exhibited low and uniform contamination. Despite the floor surface being contaminated with glassy transparent sand, no notable concentrated radiation dose rate was discerned, suggesting a lack of interaction with Cs. However, details of the painted layer on the bottom of the aqua-farming pond were not revealed.

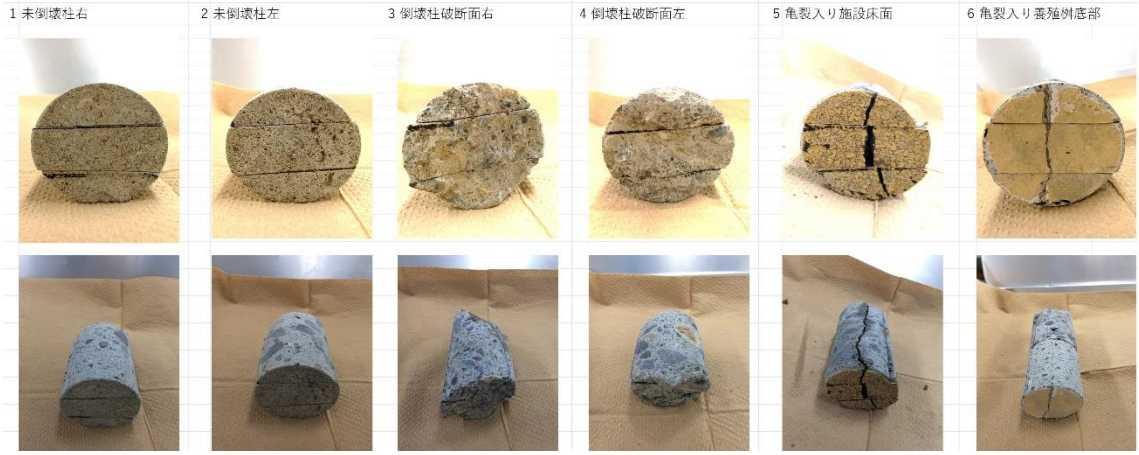

Fig. 13 Appearances of the sampled cores. 1. Upright column right, 2. Upright column left, 3. Collapsed column without cover concrete right, 4. Ibid. left, 5. Cracked floor of the facility, 6. Cracked basement of aqua-farming pond.

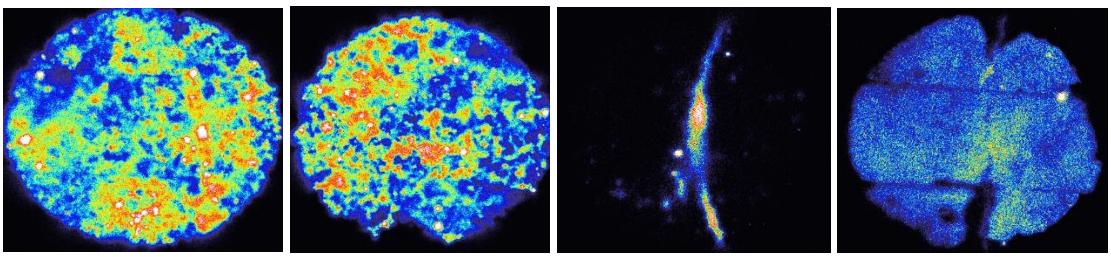

Fig. 14 Autoradiographic images of concrete core surfaces. From left to right: upright column, collapsed column, cracked facility floor, and cracked aqua-farming pond basement. The exposure time was 48 h. The contrast of the two right images is increased by a factor of 5.

https://doi.org/10.26434/chemrxiv-2024-bqr88 **ORCID:** https://orcid.org/0000-0001-5835-8636 Content not peer-reviewed by ChemRxiv. **License:** CC BY-NC-ND 4.0

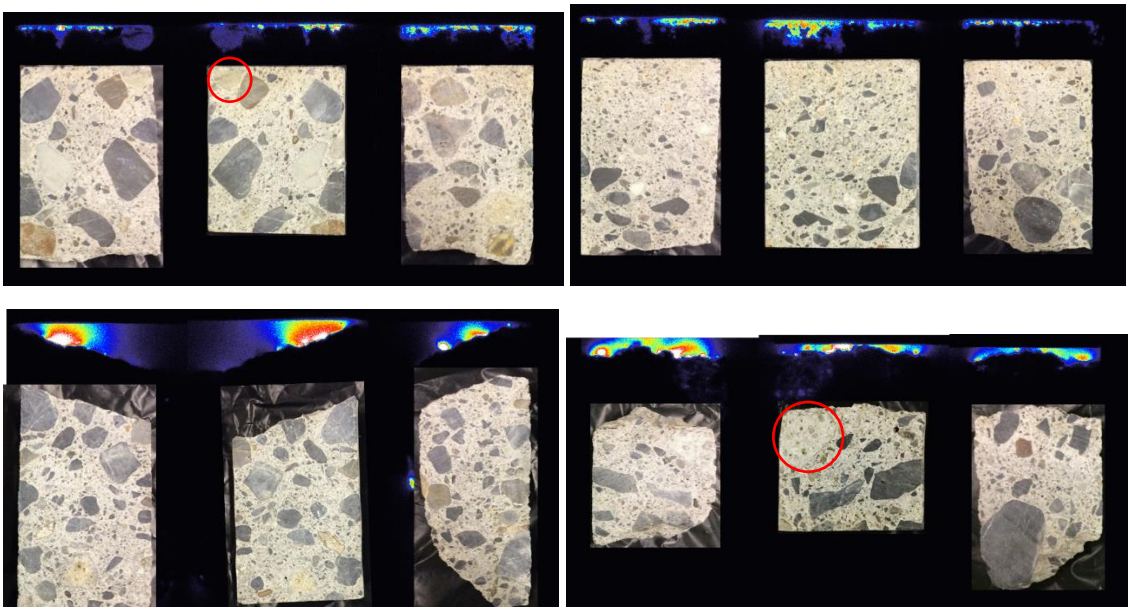

Fig. 15 IP images of cores from upright columns (upper) and from collapsed columns without concrete cover (lower). The core diameter is 47 mm. The exposure time was 48 h. Signals were detected only from the surface, and photographs of cores are overlapped on the near-surface position of IP images for better visual comparison.

IP images of core cross sections cut into three pieces are shown in Figs. 15-17. In Fig. 15, the upper section indicates two cores extracted from an upright column. These cores had flat surfaces, enabling the placement of a shield to mitigate the influence of scattered rays from the specimen surface. Radioactive Cs penetrated to a depth of a few millimeters. Weak signals were detected within the some types of aggregate particles and are particularly evident in diagrams in the upper left and second from the right of Fig. 15.

The lower portion of Fig. 15 indicates two cores obtained from a collapsed column lacking concrete cover. Radioactive contamination was confined to a superficial layer locally, and penetration into the interior was not detected during this measurement. Because of the irregular surface, it was difficult to shield the scatting signals from the surface. The localization of signal suggests that the contamination is limited to the specific light-colored aggregate as shown in Fig. 15 lower right but no or very limited contamination was observed for dark colored aggregate and cement paste part.

Fig. 16 shows an IP image of a core originating from areas with a surface coating. The top image displays a core sourced from a cracked section of a floor within the facility with a resin coating. Contamination penetrated deeply into the concrete along the cracks, with high intensity approximately 1 cm below the surface, gradually diminishing with depth. Cracks diverged at a depth of approximately 5 cm, with evident penetration along the divergent cracks. Signals were detected in the specific light-colored aggregate within the deeper part of the sample, suggesting potential penetration of radioactive Cs through the cracks into the aggregate. While localized concentrated spots were noted throughout the sample, clarity regarding whether these were contaminated during sample processing or representative of the original distribution of radioactive Cs contamination in some sand particles remains uncertain.

The lower section of Fig. 16 displays a core from a cracked area at the bottom of the aqua-farming pond. In this region, the concrete featured a 10 cm thick mortar overlying the concrete foundation, with no discernible resin layer on the surface. The material utilized for coating is not known. Here, a signal was detected from the surface layer and only a weak signal was detected along the cracks. Although the cracks traversed the entire surface mortar and reached a depth of approximately 8 cm, the Cs penetration depth was limited to a few millimeters. The reason for minimal penetration along the cracks in this area is unclear. Signals were also discerned from the aggregate deep within this core. The texture of these aggregate particles suggests a potential granite containing potassium feldspar, with radiation potentially stemming from natural K-40. Therefore, a sample of 0.12 g was ground to a 1-mm thickness using a milling machine and subsequently measured using a Ge detector for 16.5 h. While no K-40 was detected, Cs-137 was detected at 65 Bq/kg, but this is lower than the detection limit of 360 Bq/kg, hindering accurate evaluation. Additionally, a weak signal was dispersed throughout the sample, suggesting the possibility of radioactive Cs concentration in specific aggregates or sands, but further investigation is needed.

https://doi.org/10.26434/chemrxiv-2024-bqr88 **ORCID:** https://orcid.org/0000-0001-5835-8636 Content not peer-reviewed by ChemRxiv. **License:** CC BY-NC-ND 4.0

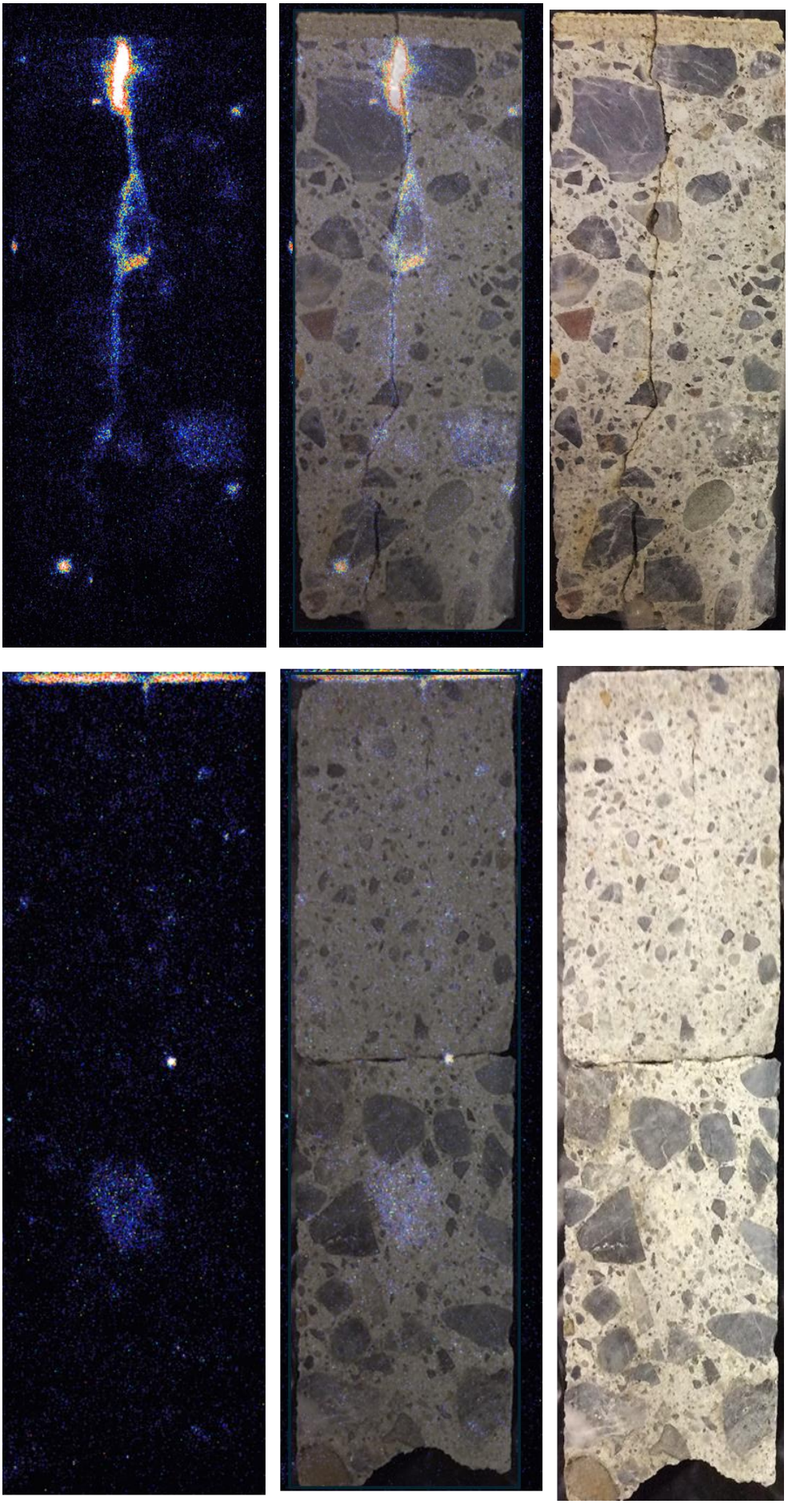

Fig. 16 IP images of a column from a cracked floor within the facility (top) and a column from the cracked basement of the aqua-farming pond (bottom). The exposure time was 48 h. The core diameter is 47 mm.

https://doi.org/10.26434/chemrxiv-2024-bqr88 **ORCID:** https://orcid.org/0000-0001-5835-8636 Content not peer-reviewed by ChemRxiv. **License:** CC BY-NC-ND 4.0

(6) Effects of carbonation and aggregates

A cross-sectional IP image of a core collected from a collapsed column (with concrete cover) during the fourth survey is shown in Fig. 17. This figure shows a photograph displaying the cut surface of the core, a photograph depicting the core after being sprayed with a phenolphthalein ethanol solution, a composite image merging the IP image with the cross-sectional photograph, and an original IP image. Concrete is neutralized by carbon dioxide gas in the atmosphere, leading to the carbonation of calcium hydroxide, a byproduct of cement hydration, to form calcium carbonate.

Fig. 18 shows the distribution of radioactivity concentration, specifically calibrated as Cs-137, derived from the IP image analysis. In all samples, radioactive Cs was notably present in neutralized regions, identifiable by their absence of red coloring. Carbonated cement paste can adsorb a significantly greater amount of Cs [17], potentially influencing the detection capabilities of IP images regarding Cs penetration into the paste area, given the tenfold increase in radioactive Cs concentration in the surface layer resulting scattering of signals. To determine whether radioactive Cs has permeated beyond the carbonated portion, the carbonated section should be removed, or grinding should be conducted, with subsequent analysis of the grinding dust for radioactivity.

The contamination level of the surface layer is presumed to have diminished over time and is estimated to have been in 100 kBq/kg order in January 2024. As shown in the lower part of Fig. 15, radioactive Cs was concentrated in the surface aggregate location, with no evident penetration detected in the concrete's interior. However, contamination by radioactive Cs occurred after the spalling of covered concrete when the concrete was not neutralized. Thus, even if Cs penetration occurred, the signal might have been too weak for detection compared to the strong signals from some aggregate positions.

Fig. 17 (middle) and Fig. 17 (lower) depict also the signals detected within the aggregates. Samples weighing 0.23 g and 0.10 g were obtained from each aggregate position using a milling machine, and both samples were evaluated using a Ge-type detector for 2.5 h and 3.5 h, respectively. The radiation concentrations of the aggregates depicted in Fig. 17 (middle and lower sections) were measured at 19 kBq/kg and 45 kBq/h, respectively. These values closely align with those obtained from the quantitative analysis through IP, as depicted in Fig. 18, indicating a greater penetration of radioactive Cs into these aggregates compared with the surrounding cement paste sections. This difference can be attributed to the Cs adsorbing capacity differences in cement paste with limited capacity and some types of aggregate with much more capacity.

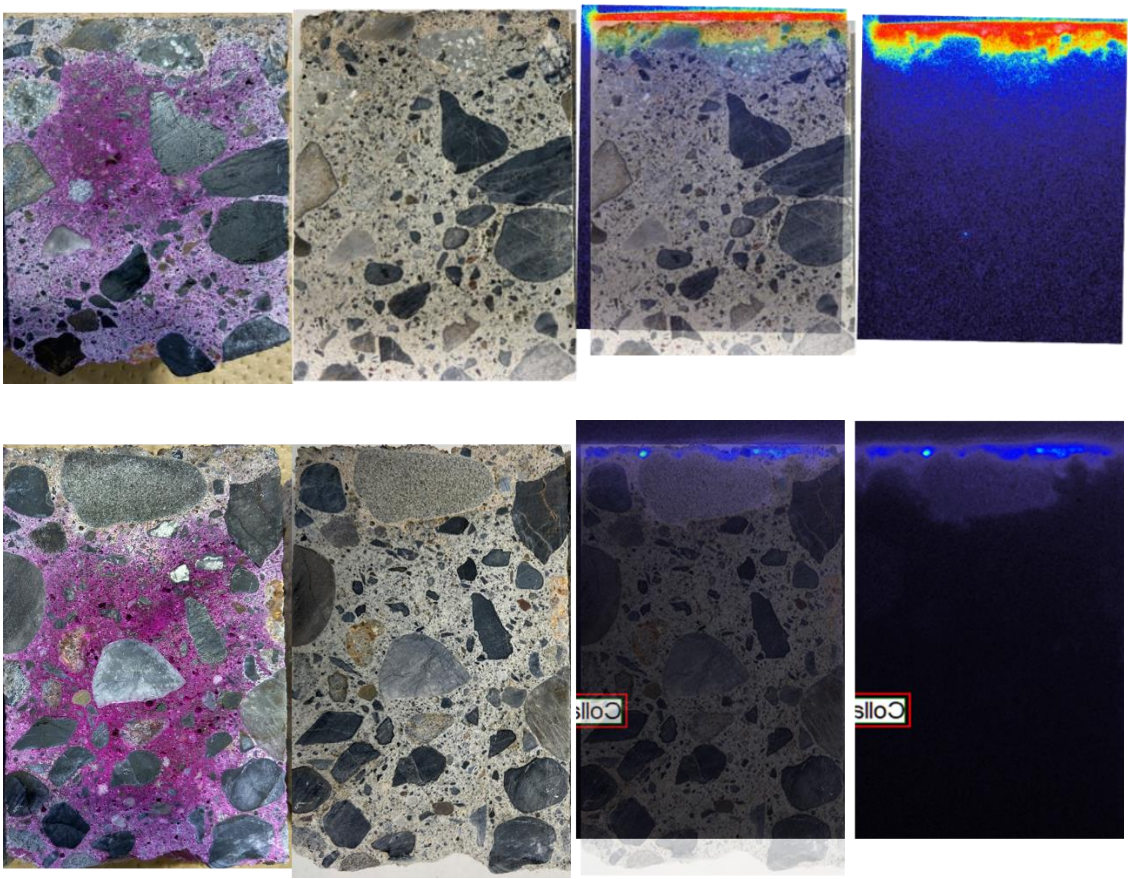

https://doi.org/10.26434/chemrxiv-2024-bqr88 **ORCID:** https://orcid.org/0000-0001-5835-8636 Content not peer-reviewed by ChemRxiv. **License:** CC BY-NC-ND 4.0

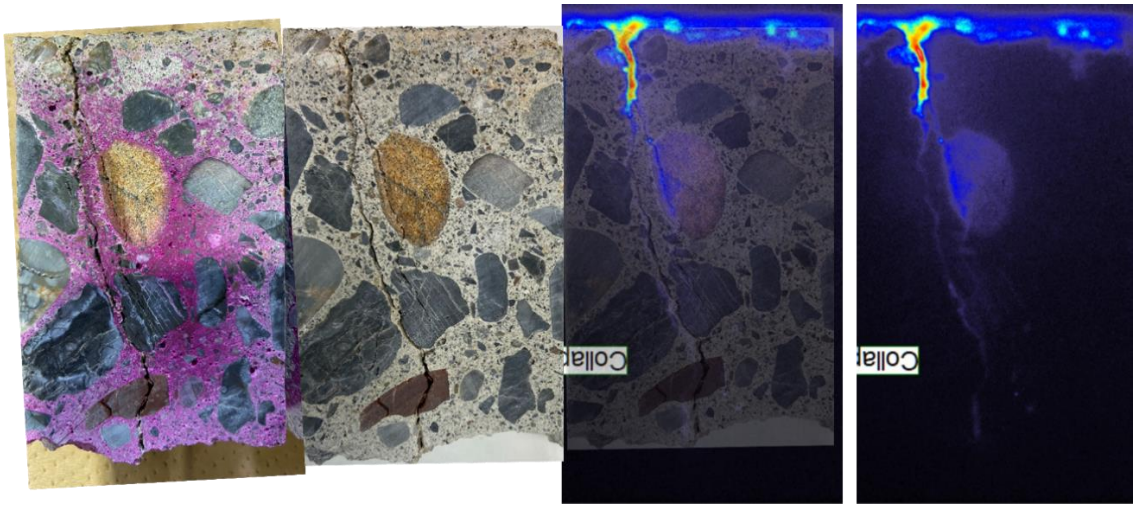

Fig. 17 IP images (right) of cores from three locations of a collapsed column with surface photographs (left). Red color indicates non-carbonated areas of concrete, highlighted by spraying with phenolphthalein solution. The exposure time was 23 h. The core diameter is 50 mm.

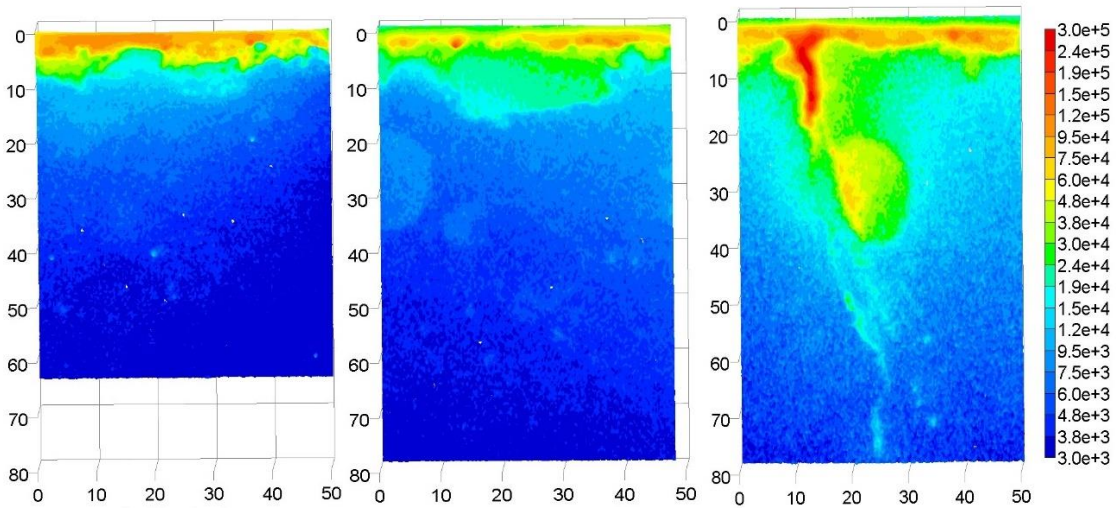

Fig. 18 Distribution of radiation concentration calibrated as Cs-137 for three samples depicted in Fig. 17, arranged from left to right and top to bottom to correspond with the panels in Fig. 17, respectively.

4. Key points to consider in predicting Cs penetration into concrete

This paper presents findings of an assessment of concrete contamination in the context of future demolition plans for the 1F concrete buildings [11], which requires estimation of contamination distribution and depth. The immediate demolition target is the superstructure of the building, which is considered to be contaminated by aerosols similar to the off-site concrete, rather than the turbine basement pit, which is directly exposed to contaminated water with various radionuclides. Therefore, the findings in this study for off-site concrete can be a reference for the contamination estimation of superstructures in 1F buildings.

Radioactive Cs is considered to be the primary contaminant of superstructure of buildings, and the radioactive contamination of on-site concrete structures is affected by several factors. First, contamination primarily occurs through the carbonated portion of cement paste, as illustrated in Figs. 15 and 17, and contamination of the non-carbonated paste is less pronounced. Although the contamination of non-carbonated paste remains unclear, carbonation level in concrete is the primary contributor to radioactive Cs contamination.

Second, IP measurements reveal penetration of radioactive Cs and its adsorption into aggregates, with Fig. 17 indicating concentration within aggregates rather than in the surrounding cement paste. Additionally, the lower portion of Fig. 17 suggests that Cs concentration occurs in some types of aggregate through cracks at shallow depths. Considering the differing Cs adsorption behavior of several types of rock as reported in previous studies [18], actual rock types used and their weathering products need to be examined.

https://doi.org/10.26434/chemrxiv-2024-bqr88 **ORCID:** https://orcid.org/0000-0001-5835-8636 Content not peer-reviewed by ChemRxiv. **License:** CC BY-NC-ND 4.0

Third, rainfall may facilitate Cs leaching from carbonated cement paste, while leaching from aggregates may be limited, as depicted in Fig. 11. Therefore, Cs adsorption on carbonated cement paste and Cs-adsorbing aggregate must be examined.

Lastly, indoor surface dose rate measurements indicated minimal contamination. Outer resin painting likely limits Cs penetration, and indoor areas are largely shielded from rainfall. Therefore, ion penetration under non-saturated conditions must be examined separately from that in rain-exposed areas, although Cs contamination is primarily caused by aerosols.

Many studies have focused on Cs penetration into cement and concrete over long time durations [19, 20, 21, 22]. This study highlights three critical factors for predicting concrete contamination by radioactive Cs not have reported: the depth of concrete carbonation, aggregate Cs adsorption, and whether the cement is exposed to water or remains dry.

5. Conclusions

The study performed surface dose rate measurements on concrete at several sites around the Fukushima Daiichi Nuclear Power Plant, radioactivity concentration assessments in a low radioactive background environment of sampled cores, and autoradiographic evaluation of core cross-sections using IP technology. The key findings of this study are as follows:

- If field, surface dose rate measurements using Geiger-Müller (GM) tubes were found to be more suitable for assessing concrete contamination than an NaI scintillator, because the latter is more susceptible to environmental radioactivity even with shielding.
- Estimating radioactivity concentration from GM tube measurements in the field yielded relatively large variations. Conversely, measurements using NaI in a low background environment could estimate surface radioactivity concentration assumed as Cs-137 with an accuracy of ±47 Bq/cm^2 in the range up to 600 Bq/cm^2.
- Contamination of rubble was observed to be higher on the top surface and lower on the sides and back surfaces of the rubble. Similarly, contamination of building columns was greater when they had collapsed and were flat-lying compared with when they were upright.
- Surface dose rates on collapsed columns outdoors halved from December 2014 to January 2024, indicating potential dissolution of radioactive Cs adsorbed on carbonated cement paste parts.
- Radioactive Cs in samples sealed and stored indoors suggesting a dry condition exhibited no migration.
- Surface contamination in concrete was observed in carbonated cement paste parts, with Cs concentration primarily by the aggregate adsorption.
- Contamination of concrete was evident in carbonated parts but only at the surface of non-carbonated parts where the concrete had collapsed and its concrete cover was spalled.
- Certain aggregate types exhibited radioactive Cs penetration throughout particles, indicating contamination levels surpassing those in surrounding cement paste.

Based on these findings, the following factors are deemed crucial for estimating contamination of the 1F concrete superstructure.

- Depth of concrete carbonation,
- Aggregate characteristics influencing Cs adsorption, and
- Environmental conditions, namely whether concrete was dry or in contact with water.

Acknowledgement

The authors gratefully acknowledge Fukushima Prefectural Research Institute of Fisheries Resources for the support in the field survey at the former Fukushima Prefecture Fish Farming Experimental Station.

References

[1] Japan Atomic Energy Agency, Airborne Monitoring in the Distribution Survey of Radioactive Substances. https://emdb.jaea.go.jp/emdb_old/en/portals/b1020201/ (Accessed on May 6, 2024)

[2] K. Yamada, Y. Takeuchi, G. Igarashi, M. Osako, Field survey of radioactive cesium contamination in concrete after the Fukushima-Daiichi nuclear power station accident, Journal of Advanced Concrete Technology, 17 (2019) 659-672. doi.10.3151/jact.17.659

[3] E.B. Farfán, S.P. Gaschak, A.M. Maksymenko, E.H. Donnelly, M.D. Bondarkov, G.T. Jannik, J.C. Marra, Assessment of (90)Sr and (137)Cs penetration into reinforced concrete (extent of "deepening") under natural atmospheric conditions,

https://doi.org/10.26434/chemrxiv-2024-bqr88 **ORCID:** https://orcid.org/0000-0001-5835-8636 Content not peer-reviewed by ChemRxiv. **License:** CC BY-NC-ND 4.0

Health Phys 101 (2011) 311-320. doi:10.1097/HP.0b013e3182103242 Corpus ID: 10237528
[4] C.V. McIsaac, C.M. Davis, J.T. Horan, D.G. Keefer, Results of analyses performed on concrete cores removed from floors and D-ring walls of the TMI-2 reactor building. Idaho, US: GEND (General public Utilities, Electric Power Research Institute, U.S. Nuclear Regulatory Commission and U. S. Department of Energy); 1984. (GEN-INF-054)
[5] K. Maeda, S. Sasaki, M. Kumai, I. Sato, M. Suto, M. Ohsaka, T. Goto, H. Sakai, T. Chigira, H. Murata, Distribution of radioactive nuclides of boring core samples extracted from concrete structures of reactor buildings in the Fukushima Daiichi Nuclear Power Plant. J. Nuclear Sci Tech, 51 (2014) 1006-1023. doi.org/10.1080/00223131.2014.915769
[6] Hokkaido University, Study on demolition of contaminated concrete and rational treatment and disposal of wastes generated, FY2018 Nuclear Energy Science & Technology and Human Resource Development Project － (2019) (in Japanese).
[7] The University of Tokyo, Quantitative Evaluation of Long-Term State Changes of Contaminated Reinforced Concrete Considering the Actual Environments for Rational Disposal － FY2022 Nuclear Energy Science & Technology and Human Resource Development Project － (2023) (in Japanese).
[8] Nagoya University, Estimation of contamination distribution in concrete members of Fukushima Daiichi NPS buildings based on mechanism-understanding of radioactive nuclides contamination of cement-based materials (Report for MEXT project mentioned in the acknowledgement) (2020) (in Japanese).
[9] K. Yamada, H. Hokora, I. Maruyama, H. Aihara, S. Tomita, Y. Tojo, K. Shibuya, Y. Hosokawa, G. Igarashi, Y. Koma, Attempts to Estimate the Amount of Contamination by Cs and Sr in Cracked Concrete Considering Realistic Contamination Conditions, Proceedings of WM Symposia, 24110, 2024
[10] Ministry of Education, Culture, Sports, Science and Technology, (1) Analysis results of γ-ray emitting nuclides and (2) Analysis results of Strontium 89, 90 (2nd distribution survey) by MEXT, Sep. 12, 2012 (in Japanese). https://radioactivity.nra.go.jp/cont/ja/docs/reps/rad-dist/sr-89-90/6213_20120912_rev20130701.pdf (Accessed on May 6, 2024)
[11] Tokyo Electric Power Company Holdings, Inc., Analysis of rubble and building demolition products etc. on 1F, 1F Technical Meeting (15th), Reference 1-1, Dec. 4, 2023. https://www.nra.go.jp/data/000461455.pdf (Accessed on May 6, 2024)
[12] Japan Atomic Energy Agency, Air dose rata in buildings, May 31, 2017. https://warp.da.ndl.go.jp/info:ndljp/pid/10375219/www.tepco.co.jp/decommision/news/data/sm/images/sv-u1-20170531-j.pdf (Accessed on May 6, 2024)
[13] Japan Atomic Energy Agency, Fukushima Daiichi Radwaste Analytical Data Library (FRAnDLi), https://frandli-db.jaea.go.jp/FRAnDLi/ (Accessed on May 6, 2024)
[14] Z. Yoshida, For Promoting Remediation of Contaminated Area ; Principle of Remediation Methods—From Tests at Date-city and Iitate-mura in Fukushima Prefecture, Journal of the Atomic Energy Society of Japan, 54, 29-33, 2012 (in Japanese).
[15] N. Osawa, K. Yamada, Y. Takeuchi, G. Igarashi, Basic experiments for the discrimination quantification of Cs-137 and Sr-90 by using an imaging plate, Proceedings of JCI, 40 (2018) 63-68 (in Japanese).
[16] K. Yamada, M. Yokokawa, T. Kawakami, Y. Sagawa, Examples of ion penetration measurements in coarse aggregates, Proceedings of JCI, 44 (2022) 382-387 (in Japanese).
[17] K. Yamada, Y. Tojo, H. Aihara, S. Tomita, H. Hokora, K. Shibuya, Y. Koma, G. Igarashi, Y. Hosokawa, I. Maruyama, Penetration of Cs and Sr into Cracked Dry Carbonated Mortar Considering the Contamination History of Fukushima Daiichi NPP, Proceedings of WM Symposia, 23068, 2023
[18] J. Hwang, W.S. Han, S. Choung, J.W. Kim, H. Suk, J. Lee, Diverse sorption capacities and contribution of multiple sorptive sites on illitic clays to assess the immobilization of dissolved cesium in subsurface environments, Journal of Hazardous Materials 441: 129973, 2023. doi.org/10.1016/j.jhazmat.2022.129973
[19] Alan Atkinson, Allan K. Nickerson, Diffusion and Sorption of Cesium, Strontium, and Iodine in Water-Saturated Cement, Nuclear Technology 81 (1988) 100-113. doi.org/10.13182/NT88-A34082
[20] K. Idemitsu, K. Kuwata, H. Furuya, Y. Inagaki, T. Arima, Diffusion Paths of Cesium in Water-Saturated Mortar, Nuclear Technology, 118 (1997) 233-241. doi.org/10.13182/NT97-A35364
[21] I. Sato, K. Maeda, M. Suto, M. Osaka, T. Usuki, S. Koyama, Penetration behavior of water solution containing radioactive species into dried concrete/mortar and epoxy resin materials, Journal of Nuclear Science and Technology 52 (2015) 580-587. doi.org/10.1080/00223131.2014.963725
[22] M. García-Gutiérrez, T. Missana, M. Mingarro, J. Morejón, J.L. Cormenzana, Cesium diffusion in mortars from different cements used in radioactive waste repositories, Applied Geochemistry, 98 (2018) 10-16. doi.org/10.1016/j.apgeochem.2018.09.001

https://doi.org/10.26434/chemrxiv-2024-bqr88 **ORCID:** https://orcid.org/0000-0001-5835-8636 Content not peer-reviewed by ChemRxiv. **License:** CC BY-NC-ND 4.0